Optimizing and Predicting CHF in Spray Cooling of a Square Surface

I. Mudawar
Professor and Director.

K. A. Estes
Graduate Student.

Boiling and Two-Phase Flow Laboratory,
School of Mechanical Engineering,
Purdue University,
West Lafayette, IN 47907

Spray cooling of a hot surface was investigated to ascertain the effect of nozzle-to-surface distance on critical heat flux (CHF). Full cone sprays of Fluorinert FC-72 and FC-87 were used to cool a 12.7 × 12.7 mm² surface. A theoretical model was constructed that accurately predicts the spray's volumetric flux (liquid volume per unit area per unit time) distribution across the heater surface. Several experimental spray sampling techniques were devised to validate this model. The impact of volumetric flux distribution on CHF was investigated experimentally. By measuring CHF for the same nozzle flow rate at different nozzle-to-surface distances, it was determined CHF can be maximized when the spray is configured such that the spray impact area just inscribes the square surface of the heater. Using this optimum configuration, CHF data were measured over broad ranges of flow rate and subcooling, resulting in a new correlation for spray cooling of small surfaces.

1 Introduction

Sprays can be formed either by supplying liquid at high pressure through a small orifice (pressure spray) or by breaking the liquid with the aid of a high-pressure supply of air (atomized spray). The present study is concerned with pressure sprays that simplify cooling by requiring a single (pure) working fluid.

Spray cooling has long been employed in the quenching of metals upon exit from a high-temperature furnace, and many studies exist in the literature for predicting spray heat transfer for those situations (e.g., Watchers et al., 1966; Bolle and Moureau, 1976; Moriyama et al., 1987). Since furnace temperatures typically correspond to the film boiling regime, these studies are not applicable to situations involving removal of high heat fluxes at relatively low surface temperatures such as cooling of supercomputer electronics, avionics, x-ray medical devices, and lasers—devices for which the findings of the present study are intended.

Spray and jet cooling are often considered competing options in these types of application. A major disadvantage to jet cooling is that the large concentration of heat removal within the impingement zone causes relatively large temperature gradients within the cooled surface, which can result in catastrophic failure of certain temperature sensitive devices. This problem can be partially alleviated by employing an array of jets to cool a single device; however, interference between neighboring wall jets emanating from the impingement zones of the individual impinging jets greatly complicates coolant flow. Two-phase jet cooling is further complicated by an inability to sustain much phase change in the wall jet. To release the vapor produced at the surface, wall jets tend to separate from the surface due to the vapor momentum perpendicular to the surface. In fact, CHF in jets is often encountered even with an abundance of liquid in the wall jet (Monde et al., 1980).

Sprays, on the other hand, utilize the momentum of liquid entering the spray nozzle to induce breakup into fine drops, which impinge individually upon the heated surface. Not only does the breakup increase the surface area to volume ratio of the liquid, but it also helps produce a more uniform spatial distribution of heat removal both in the single-phase and nucleate boiling regimes. Another key feature of spray cooling is delaying liquid separation from the surface during vigorous boiling. By bombarding the entire surface with drops, the momentum of the individual drops is more effective at resisting the momentum of vapor perpendicular to the surface than a wall jet. Simply stated, the liquid film deposited upon the heater surface in the case of jet cooling is "anchored" to the surface only at the impingement zone and is, therefore, susceptible to breakdown and separation over much of the heater surface; the liquid film in the case of spray cooling in anchored to the entire surface.

Despite these advantages, spray cooling remains less popular for cooling of low-temperature, high heat flux devices for several reasons. Breakup of the liquid flow to fine drops demands relatively high pressures, which may not be desirable in certain situations, and the small size of the spray orifice increases the likelihood of clogging, which could lead to eventual surface burnout. Furthermore, seemingly identical nozzles machined with close tolerances often fail to produce identical spray patterns; careful testing of nozzle patterns is essential where predictable and repeatable cooling performance is a must (Hall and Mudawar, 1995). But the single most important reason for the limited use of spray cooling in low-temperature, high heat flux situations is undoubtedly the lack of understanding of the mechanisms of boiling, especially CHF, and the absence of useful heat transfer correlations that can be employed over broad ranges of spray parameters.

Spatial Variations in Spray Cooling. The pressure (liquid-only) sprays commonly used in cooling applications are categorized as either full-cone sprays or flat sprays, which possess circular and oval spray impact areas, respectively. Mudawar and Deiters (1994) investigated the spatial variation of the heat transfer coefficient across the impact area in both full-cone and flat water sprays. They also measured the spatial variations of the key hydrodynamic parameters of the spray just prior to impact. These include volumetric flux, Q'', mean drop velocity, U_m, and Sauter mean diameter, d_{32}. Both Q'' and U_m are measured in units of velocity, the former being the volume flow rate of liquid impacting an infinitesimal portion of the impact area divided by the area of the same portion. Mudawar and Deiters observed that while U_m was virtually constant for the entire spray impact area, the heat transfer coefficient peaked at the center of the impact area and decayed gradually away from the center, becoming negligible just outside of the impact

Contributed by the Heat Transfer Division for publication in the JOURNAL OF HEAT TRANSFER. Manuscript received by the Heat Transfer Division January 10, 1995; revision received April 2, 1995. Keywords: Boiling, Electronic Equipment, Sprays/Droplets. Associate Technical Editor: T. W. Simon.

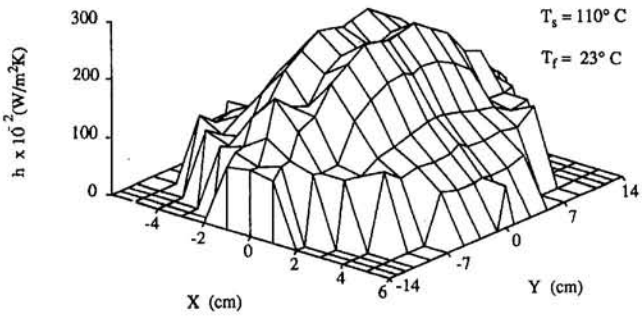

Fig. 1 Variation of heat transfer coefficient across spray impact area

area as shown in Fig. 1. This spatial distribution followed essentially the distribution of volumetric flux, Q'', across the impact area.

In fact, the dimensionless correlations developed by Mudawar and Valentine (1989) reveal what was suggested earlier by Toda (1972): The proper scaling velocity for heat transfer correlations near CHF is Q'' not U_m, and the scaling length is d_{32}. Increasing Q'' for water sprays ameliorated heat transfer, while increasing drop diameter adversely affected CHF; smaller drops yielded better cooling.

A key reason why Q'' and not U_m is the appropriate scaling velocity in correlating CHF data is that the latter fails to account for the commutative effect of multiple drop impact; i.e., its magnitude has no bearing on the number of drops impacting the surface per unit area per unit time. In fact, different sprays can possess equal drop velocities but vastly different volumetric fluxes.

Unlike the studies by Mudawar and Valentine and by Mudawar and Deiters, which resulted in correlations for a small heater positioned in a much larger spray impact area, the present study is concerned with spray boiling and CHF from a square heater almost entirely impacted by the spray. Key objectives of the present study are to

1 develop a better understanding of how volumetric flux influences cooling performance for the full cone sprays commonly employed in low-temperature, high heat flux applications;
2 optimize nozzle-to-surface distance in order to maximize CHF; and
3 develop a CHF correlation that precludes having to perform costly spray drop sizing experiments.

2 Experimental Facility

Flow Loop and Test Chamber. The working fluid (FC-72 or FC-87) was deaerated and conditioned to the desired operating pressure and temperature using the flow loop shown in Fig. 2(*a*). The spray was formed within the test chamber of the loop. A magnetically coupled centrifugal pump transferred the fluid from a reservoir situated beneath the test chamber through the loop components, which included three flat plate heat exchangers, a carbon filter, a flow-through electrical heater, and one of two rotameters. Two of the flat plate heat exchangers removed essentially the heat added by the pump, while fine tuning of the liquid temperature upstream of the test chamber was accomplished by heat addition in the flow-through electrical heater and additional heating or cooling via the third heat exchanger inside which water was circulated through a constant temperature bath.

A pressure gage was situated just upstream of the spray nozzle and another connected directly to the test chamber. Pressure difference across the nozzle was used to correlate Sauter mean diameter data, while the test chamber pressure was the reference for determining the saturation temperature and associated properties used in correlating CHF data. Uncertainties in the pressure measurements were determined from the pressure gage manufacturer specifications to be less than 0.5 percent, which was also confirmed by calibration. Uncertainties in the spray flow rate measurement resulting from fabrication tolerances, effects of temperature changes on the density and viscosity of the fluid, as well as the expansion and contraction of the rotameter parts, were estimated from the manufacturer specifications at 1.6 percent; this value was also confirmed by calibration.

Inside the chamber, liquid exiting the nozzle impinged upon the test heater and drained directly into the loop reservoir, as shown in Fig. 2(*b*). Any vapor produced within the chamber was recovered by a condensing coil situated within the chamber itself. A micrometer translation platform mounted atop the test chamber enabled precise positioning of the spray nozzle relative the test heater's surface. As shown in Fig. 3(*a*), the impingement surface, which measured 12.7 × 12.7 mm^2, was fabricated from oxygen-free copper. Heat was dissipated to the impingement surface by a thick film electrical resistor, which was soldered to the underside of the copper block as shown in Fig.

Nomenclature

A = area defined along the heater's surface
A' = area defined along a spherical surface
c_p = specific heat at constant pressure
d_i = middle diameter of ith class of drops
d_0 = nozzle orifice diameter
d_{32} = Sauter mean diameter (SMD)
H = nozzle-to-surface distance
h_{fg} = latent heat of vaporization
L = heater length (12.7 mm)
n_i = number of drops in ith class
P = test chamber pressure
ΔP = pressure drop across spray nozzle
q = electrical power input to heater
q'' = heat flux based on entire square heater area = q/L^2
q''_m = critical heat flux based on entire square heater area = q/L^2 (at CHF)
$q''_{m,p}$ = local critical heat flux at outer edge of impact area
$q''*$ = dimensionless CHF
Q = total volumetric flow rate of spray
Q'' = local volumetric flux (liquid volume per unit area per unit time)
$\overline{Q''}$ = average volumetric flux over spray impact area = $Q/(\pi R^2)$ (or $Q/(\pi L^2/4)$ for an optimized spray)
Q_i = flow rate incident at target (insert)
Q_s = flow rate incident on heater surface
Q''_{sp} = uniform volumetric flux along a spherical surface
r = radial coordinate
R = radius of spray impact area
R_i = target (insert) radius
T = temperature
T_f = spray inlet temperature
ΔT_{sub} = liquid subcooling at nozzle inlet = $T_{sat} - T_f$
ΔT_w = surface-to-liquid temperature difference = $T_w - T_f$
U_m = mean drop velocity
We = spray Weber number
γ = integration angle in volumetric flux distribution model
θ = spray cone angle
μ = viscosity
ρ = density
σ = surface tension

Subscripts

f = liquid
g = vapor
sat = saturation
sub = subcooling
w = heater surface condition

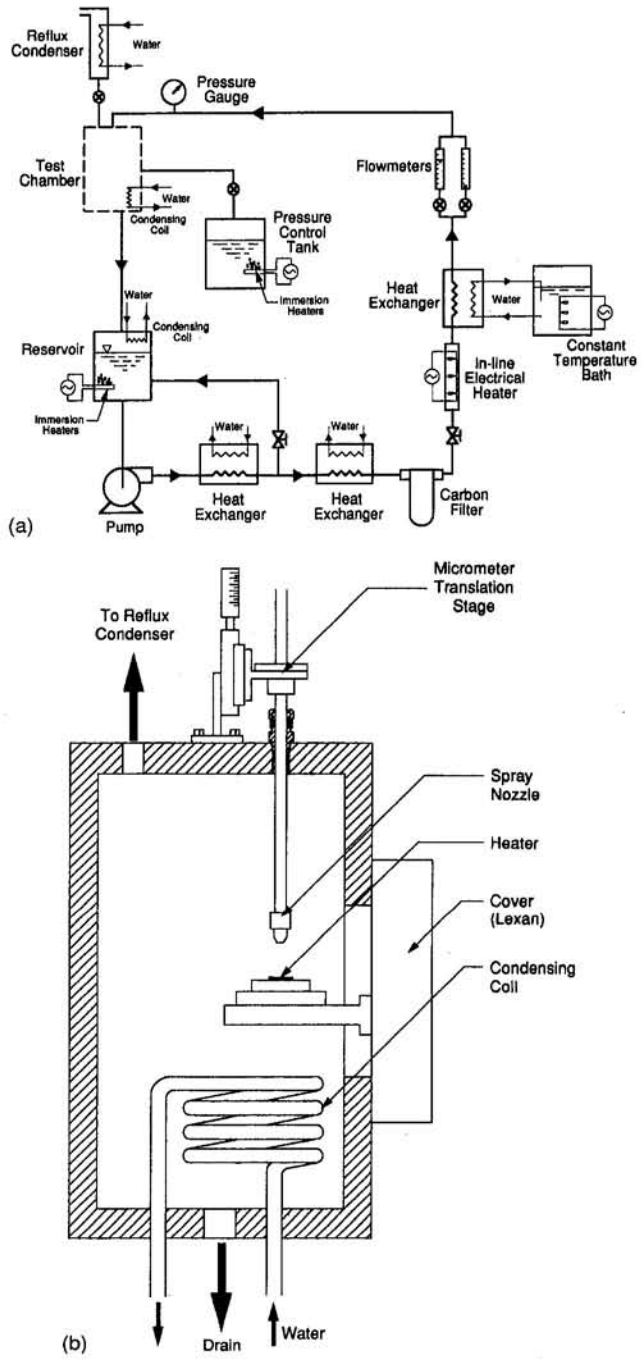

Fig. 2 Schematic of (*a*) flow loop and (*b*) test chamber

3(*b*). The heater assembly was insulated on all surfaces save the impingement surface with G-7 fiberglass plastic.

Uncertainties in the measurement of electrical power input to the thick film resistor due to the Watt transducer and the resistance of the thick film resistor's lead wires was estimated at 1.0 percent. Another source of uncertainty in the measurement of heat flux was the heat loss from boundaries other than the sprayed surface. A numerical scheme provided a conservative estimate for this heat loss. This scheme is based on the assumption that the heat transfer coefficient on the plastic surface surrounding the sprayed heater surface equals the heat transfer coefficient on the sprayed surface itself. To calculate this heat transfer coefficient, perfect contact was assumed between the heater and all surrounding plastic material. A two-dimensional finite element model was developed, assuming the heat transfer coefficient was equal to the electrical power divided by the product of measured temperature difference and sprayed area. The model was then refined by subtracting from the electrical power the heat loss estimated from the first calculation. Further iteration resulted in a heat loss estimate for a given electrical power input. This heat loss was adjusted for heat loss through the two transverse planes to account more accurately for three-dimensional heat loss. This numerical technique was employed for power input levels corresponding to the single-phase and nucleate boiling regimes, resulting in values smaller than 4.5 and 1.0 percent, respectively.

Operating Procedure. Prior to each test, the heater module was removed from the test chamber and the heater surface was polished using Happich Simichrome polishing paste. A cotton applicator dipped in methanol was then used to remove any residue left on the surface by the polish.

The fluid was carefully deaerated after the heater module was mounted inside the test chamber. Immersion heaters located in

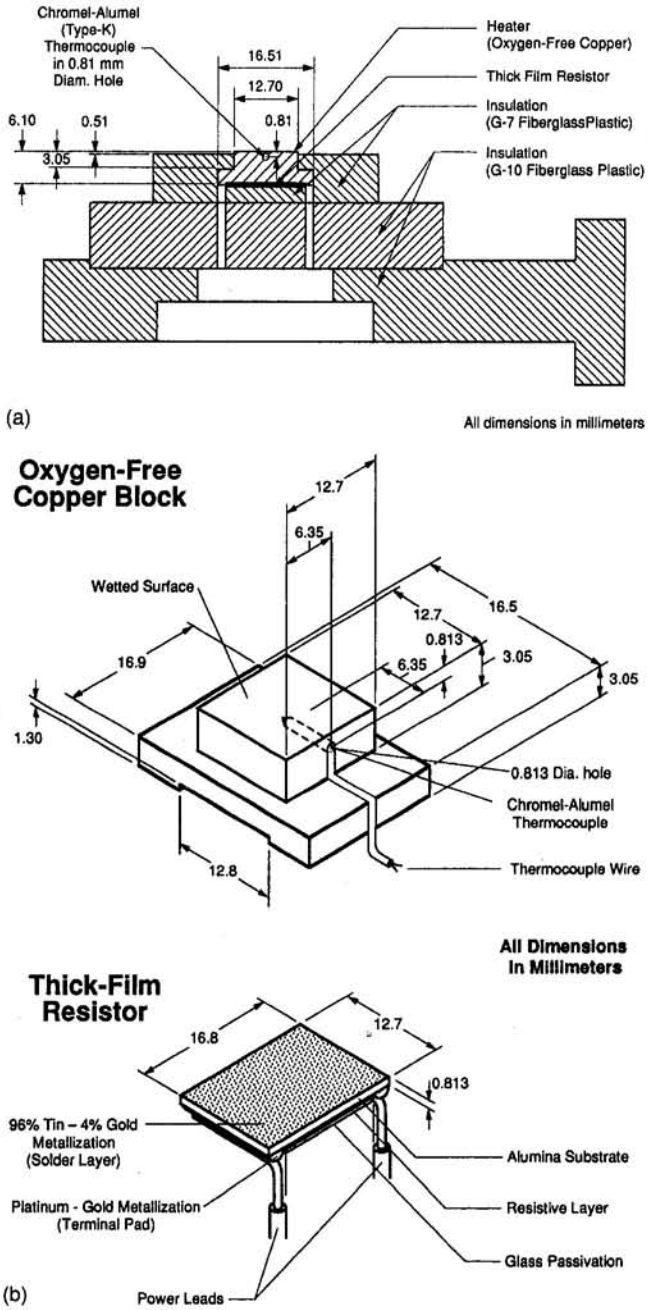

Fig. 3 Construction of (*a*) heater module and (*b*) test heater

the reservoir were used to boil the liquid, forcing the vapor produced and any dissolved noncondensible gases to exit through a reflux condenser connected to the top of the test chamber. Cold water circulating through the reflux condenser recovered the pure vapor while the noncondensible gases escaped freely to the ambient. After about 15 minutes of vigorous boiling in the reservoir, the pump was started and the deaeration proceeded for an additional 15 minutes as the fluid circulated through the loop.

Upon completion of the deaeration, the line connecting the test chamber to the reflux condenser was closed off to seal the loop completely. Pressure in the chamber was then adjusted to, and maintained at 1.03 bar (15 psia), by controlling vapor production inside the test chamber. The vapor production could be increased by increasing electrical power to immersion heaters inside a pressure control tank connected to the test chamber, or decreased by increasing the flow of water through the condensing coil inside the test chamber itself.

Boiling curves were obtained by raising the voltage across the heater's thick film resistor in small increments, using an autotransformer, and recording both the heat flux at the heater surface and the surface temperature. A Keithley 500 data acquisition system monitored and recorded both the power supplied to the heater, via a watt transducer, and temperatures throughout the loop, including the heater and nozzle inlet. The boiling data were recorded only after the heater temperature reached steady state. The power increments were reduced to less than 1.0 W/cm^2 as CHF was approached in order to both preclude premature occurrence of CHF and ensure accurate CHF measurement.

CHF was identified when the heater thermocouple detected a sudden unsteady rise in the heater temperature. Repeatability of CHF data throughout the study was ensured by running tests under identical conditions weeks and often months apart. No two such data points departed from one another by more than 5 percent. This repeatability was the result of the consistent operating procedure and the careful surface preparation, including the use of the polishing paste to help prevent the formation of an oxide layer during a given test.

3 Spray Sampling Techniques

As indicated earlier, two types of spray are commonly used in industry: air-assist (atomized) sprays and pressure (liquid-only) sprays. It is extremely difficult to publish generic fundamental studies on atomized sprays because their nozzles are available in a large variety of complex designs. With the exception of a few specialized nozzles (e.g., spiral-shaped, acoustically controlled), pressure sprays are generally available in a simple basic design. The applications for which the findings of the present study are intended (e.g., cooling of electronic and laser devices) preclude mixing of air with the liquid coolant, which explains why only pressure sprays were employed. To the authors' knowledge, Spraying Systems' full cone series nozzles are the industry's standard for sprays intended to provide full coverage over a circular impact area. The basic and generic design of these nozzles, and their popularity are all reasons behind their use in the present study. The full cone spray is produced by a simple stationary vane inside the nozzle, which induces turbulence in the liquid prior to exiting the orifice in order to promote liquid break-up.

Hall and Mudawar (1995) demonstrated experimentally that repeatability in spray impact pattern and cooling performance requires adherence to specific operation guidelines. These guidelines were strictly followed in the present study. They include: (a) avoiding brass nozzles and using nozzles made from erosion and corrosion resistant materials (only stainless steel nozzles were used in the present study); (b) testing nozzles periodically to make sure flow rate and spray angle are repeatable; (c) visually examining the spray pattern during operation for any irregularities (unsymmetric spray pattern, deflected spray, dented orifice); and (d) using a high-purity fluid and installing a small particle filter upstream of the nozzle. As an added precaution, the same nozzles used for drop diameter measurements were also used in the heat transfer measurements.

The spray heat transfer data measured in the present study were correlated with respect to the spray Weber number as proposed by Mudawar and Valentine (1989), the ratio of spray momentum to the surface tension forces exerted upon the spray drops:

$$\mathrm{We} = \frac{\rho_f Q''^2 d_{32}}{\sigma}. \tag{1}$$

The Weber number can be based on either local or average values of volumetric flux. The local volumetric flux, Q'', is the volumetric flow rate for an infinitesimal portion of the impact surface divided by the area of the same portion. Another convenient measure of spray flux is the average volumetric flux, $\overline{Q''}$, which can be readily determined by dividing the total volumetric flow rate of the spray by the portion of the surface directly impacted by the spray, the so called spray impact area. Of course, sprays with the same values of $\overline{Q''}$ can yield different cooling performances, depending upon the spatial distribution of Q''. This important issue will be discussed in detail in the next section.

The Sauter mean diameter (SMD), d_{32}, used to calculate the spray Weber number, Eq. (1), is defined as the diameter of the drop with a volume-to-surface area ratio that equals the volume to surface area ratio of the entire spray:

$$d_{32} = \frac{\Sigma\, n_i d_i^3}{\Sigma\, n_i d_i^2}, \tag{2}$$

where n_i represents the number of drops in a size class i and d_i is the middle diameter of this ith class. Estes (1994) measured drop diameters for the full cone spray nozzles employed in the present study using FC-72 and water using a Phase Doppler Particle Analyzer (PDPA). Adopting a correlation form recommended by Lefebvre (1989) for liquid breakup, Estes reduced his own full cone spray data according to the equation

$$\frac{d_{32}}{d_0} = 3.07\left[\frac{\rho_g^{1/2}\Delta P d_0^{3/2}}{\sigma^{1/2}\mu_f}\right]^{-0.259} \tag{3}$$

with a mean absolute error of 12.4 percent, where d_0 and ΔP are the diameter of the nozzle orifice and the nozzle pressure drop, respectively.

As shown in Fig. 4, when the nozzle is remote from the heater surface, the fraction of liquid leaving the nozzle that impacts the surface is a function of spray angle, θ, nozzle-to-surface distance, H, and heater length, L. To measure this fraction experimentally, a spray sampler fitted with a graduated cylinder (collector) was fabricated. As shown in Fig. 5(a), the sampler possessed a knife-edged inlet with a sampling area equal to the heater surface area, 12.7 × 12.7 mm^2. The sampler was mounted in the heater flange itself with its inlet positioned at the exact location of the heater. Mounted above the sampler was a quick-release shading plate, which deflected the flow from the collector until the spray became fully developed and the operator was ready to commence sampling. An O-ring glued to the underside of the shading plate proved effective at preventing liquid that accumulated on the plate's underside from dripping into the collector. During the measurement, the shading plate was quickly pulled back, allowing liquid to accumulate in the collector to a preset volume, and then quickly repositioned to shelter the sampling area. The volumetric flow rate incident upon the heated surface was estimated as the volume collected divided by the product of sampling area (heater area) and fill time.

Since the spray's volumetric flux is not uniform across the heated surface area, the spray sampler shown in Fig. 5(a) could

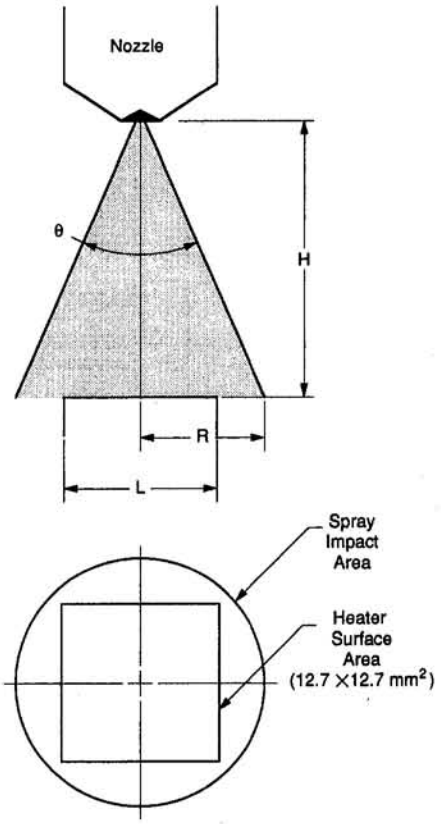

Fig. 4 Nozzle-heater configuration

not measure the spatial distribution of volumetric flux. This distribution was inferred with the aid of inserts, shown in Fig. 5(*b*), which were slid into the square opening of the original sampler as illustrated in Fig. 5(*c*). The three different sized circular openings of these inserts enabled measurement of flow rate over sampling areas smaller than the heater surface area.

4 Volumetric Flux Distribution Model

As indicated by Mudawar and Deiters (1994), volumetric flux is not uniform across the spray impact area. A model is, therefore, developed to predict how the spray flow rate is distributed across the heated surface. The model, which is intended for the full breakup region of the spray away from the orifice, is based on the assumption that the total spray flow rate, Q, is uniformly distributed over any spherical surface centered at the spray orifice (i.e., the orifice represents a uniform point source for the sprayed liquid) and bound by the spray cone angle, θ. The validity of this assumption will become apparent from the experimental results discussed later.

As the spray impacts a flat surface located a distance H from the orifice, the uniform volumetric spray flux along the spherical surface of radius H produces a volumetric flux on the impact surface, which decreases radially from the center of the impact surface. As shown in Fig. 6, a differential area, dA', along the spherical surface is given by

$$dA' = 2\pi H^2 \sin \gamma d\gamma. \tag{4}$$

Integrating γ between 0 and $\theta/2$ yields the area of the spherical surface bound by the spray angle,

$$A' = 2\pi H^2[1 - \cos(\theta/2)]. \tag{5}$$

Since a uniform volumetric spray flux is assumed over the spherical surface area A', this flux can be defined as

$$Q''_{sp} = \frac{Q}{2\pi H^2[1 - \cos(\theta/2)]}. \tag{6}$$

The projection of dA' upon the flat impact surface is another differential area, dA, which can be defined as

$$dA = \pi(H \tan(\gamma + d\gamma))^2 - \pi(H \tan \gamma)^2$$

$$= 2\pi H^2 \frac{\sin \gamma}{\cos^3 \gamma} d\gamma. \tag{7}$$

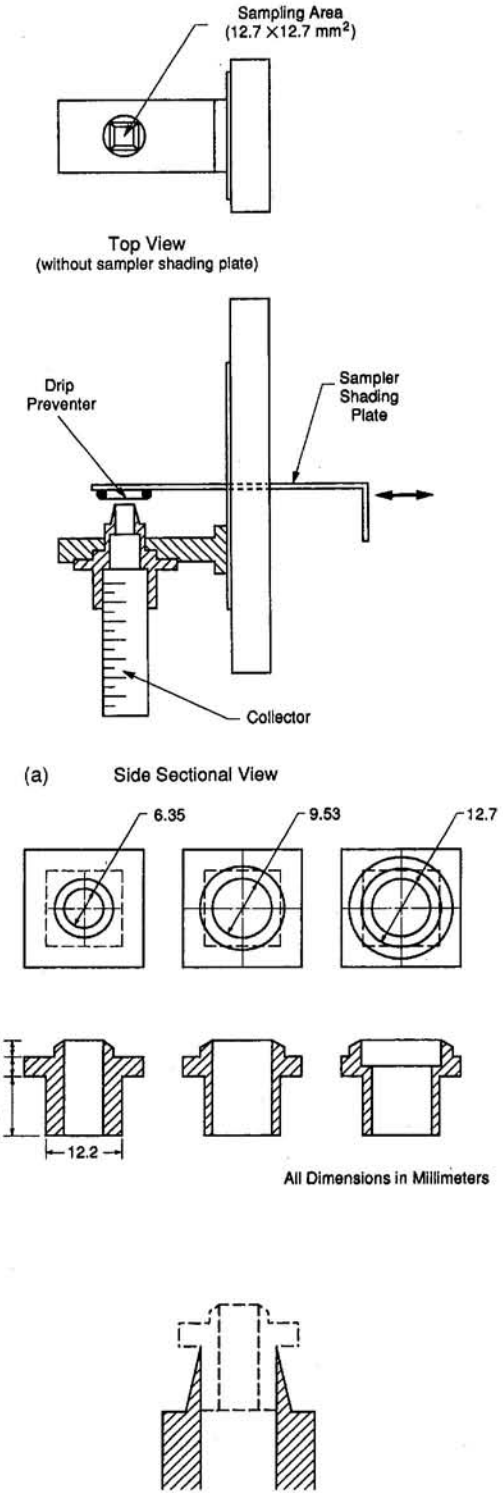

Fig. 5 Construction of (*a*) spray sampler and (*b*) inserts used for determination of volumetric flux distribution, and (*c*) placement of inserts in sampler

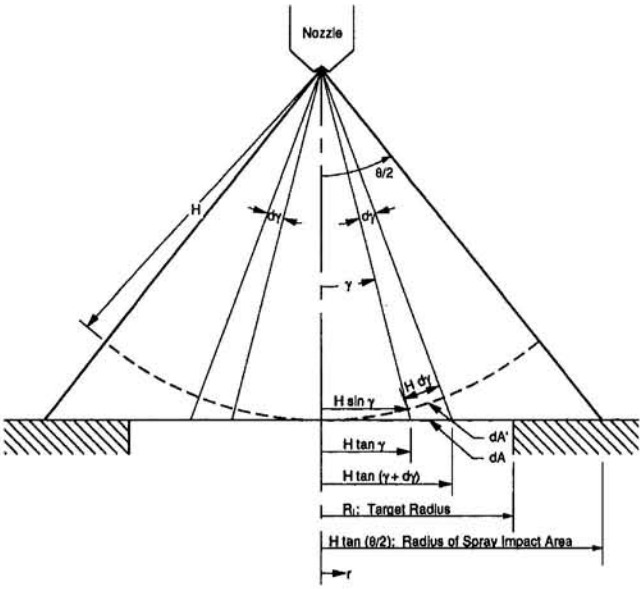

Fig. 6 Geometry used in development of volumetric flux distribution model

Thus, the spray volumetric flux along the impact surface is given by

$$Q'' = Q''_{sp}\frac{dA'}{dA} = \frac{Q}{[1-\cos(\theta/2)]}\cdot\frac{1}{2\pi H^2\cos^3\gamma}$$

$$= \frac{1}{2}\left[\frac{Q}{\pi(H\tan(\theta/2))^2}\right]\left[\frac{\tan^2(\theta/2)}{1-\cos(\theta/2)}\right]$$

$$\times\frac{1}{\left[1+\left(\frac{r}{H}\right)^2\right]^{3/2}}. \quad (8)$$

A small circular target of radius R_i centered on the impact surface will receive a flow rate

$$Q_i = \int_0^{R_i} Q''2\pi r dr. \quad (9)$$

Dividing Q_i by the total spray flow rate, Q, gives the fraction of the flow rate impacting the target.

$$\frac{Q_i}{Q} = \frac{1}{1-\cos(\theta/2)}\left[1-\frac{1}{\sqrt{1+\left(\frac{R_i}{H}\right)^2}}\right]$$

$$\text{for} \quad R_i < H\tan(\theta/2). \quad (10)$$

Targets with $R_i > H\tan(\theta/2)$, on the other hand, will capture the entire flow rate.

The flow rate captured by any of the inserts shown in Fig. 5(*b*) should then equal Q_i as defined in Eqs. (9) and (10). Figure 7 shows that the volumetric flux predicted by Eq. (8) decreases from a maximum along the spray axis to roughly one half of the maximum toward the outer edge of the impact area. Figure 8 illustrates, for Fluorinert FC-87 (only FC-87 was used in verifying the volumetric flux distribution model), the favorable agreement between measured and predicted ratios of flow rate captured by the insert to total spray flow rate, Eq. (10).

These results prove the fraction of the spray flow rate received by a target can be determined purely from geometric arguments. This fraction equals unity for $H \le R_i/\tan(\theta/2)$. This conclusion is crucial to the optimization of heat transfer from spray-cooled targets, especially near CHF. Maximum utilization of the spray flow rate is achieved when $H \le R_i/\tan(\theta/2)$. On the other hand, a very small nozzle-to-surface distance would concentrate the spray impact area over only a small central portion of the heated surface, depriving the surrounding surface from direct impact by the spray drops. It is, therefore, of paramount importance to determine the nozzle-to-surface distance that would yield the highest CHF. This issue is further complicated with square targets that possess corner regions that are less adequately cooled than the center. The next section will examine the problem of optimizing the nozzle-to-surface distance for a square target.

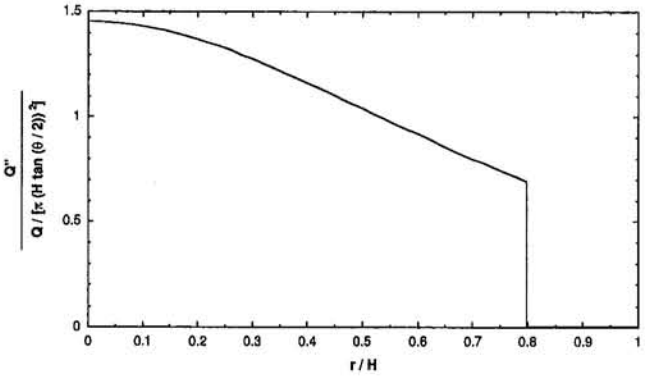

Fig. 7 Predicted distribution of volumetric flux

5 Optimization of Nozzle-to-Surface Distance and Correlation of CHF Data

CHF measurements were repeated at different nozzle-to-surface distances while maintaining the same flow rate. Figure 9 shows the ratio of CHF measured at a given nozzle-to-surface distance to the maximum CHF measured over the entire range of distances, plotted against $H\tan(\theta/2)/(L/2)$. Also shown in the same figure is the ratio of flow rate captured by the sampler without an insert (i.e., with a sampling area equal to the heater surface area) to the total spray flow rate. The largest critical heat flux seems to occur near the point where the spray just inscribes the square heated area, i.e., $H = (L/2)/\tan(\theta/2)$.

These results reveal that when the spray impact area is small (i.e., for small nozzle-to-surface distances), only a small fraction of the heated area is directly impacted by the spray drops, yielding small CHF values. CHF also decreases when the nozzle-to-surface distance is increased past the point of heated area inscription by the spray because a fraction of the liquid leaving

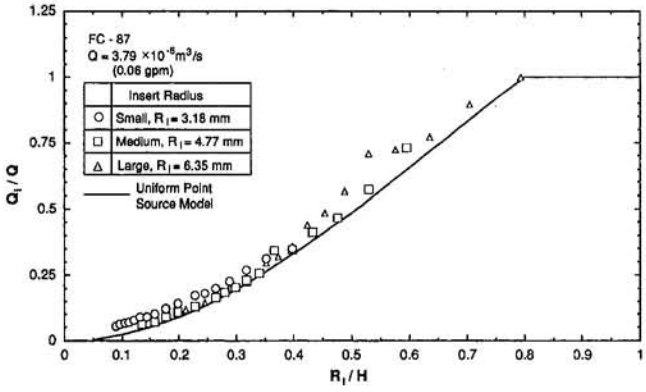

Fig. 8 Comparison of the model predictions of flow rate collected using the inserts with experimental data

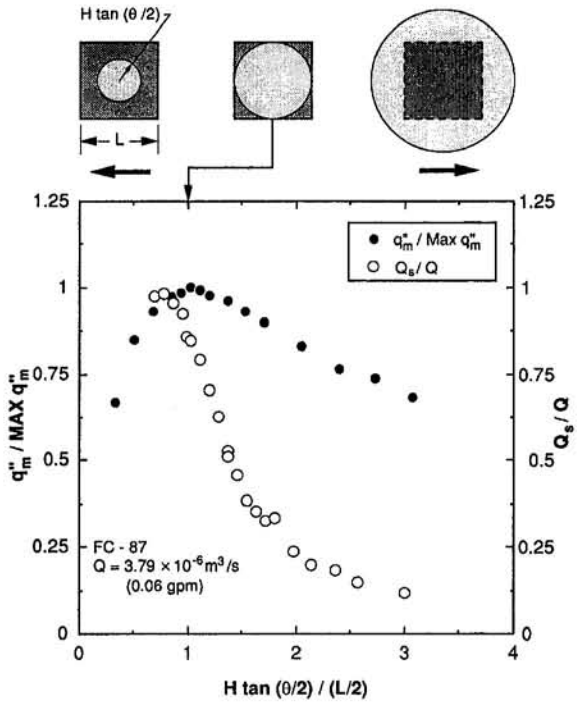

Fig. 9 Optimization of nozzle-to-surface distance for maximum CHF

the nozzle would be wasted. It is, therefore, recommended that a spray intended to cool a square heated surface be configured such that its impact area just inscribes the heater surface. Not only does this configuration maximize CHF, but it is also very simple to accomplish since it requires knowledge of only spray angle and heater size. This configuration was, therefore, utilized and maintained throughout the data base used to develop the CHF correlation.

Katto and co-workers (see Monde et al., 1980) proved that CHF data for most external flow boiling systems can be correlated according to a single dimensionless equation in terms of density ratio, Weber number, and Jacob number, using empirical coefficients and exponents. Mudawar and Valentine (1989) replaced the characteristic velocity and characteristic length in the general Katto equation by volumetric flux and Sauter mean diameter for spray cooling systems. They correlated CHF for a small circular heater situated in a large impact area according to the equation

$$\frac{q''_{m,p}}{\rho_g Q'' h_{fg}} = f\left[\frac{\rho_f}{\rho_g}, \frac{\rho_f Q''^2 d_{32}}{\sigma}, \frac{\rho_f c_{p,f} \Delta T_{sub}}{\rho_g h_{fg}}\right], \qquad (11)$$

where $q''_{m,p}$, Q'', and d_{32} are all based on local conditions within the spray impact area. The lowest CHF values were attained at the outer edge of the impact area, where Q'' is lowest; CHF was negligible outside the impact area.

Subcooling played an important role in the present study. Figure 10 shows that CHF increased monotonically with increasing subcooling in accordance with trends observed with most flow boiling systems. The subcooling was defined as the saturation temperature corresponding to the measured test chamber pressure minus the liquid temperature just upstream of the nozzle. Neglecting any significant temperature drop across the nozzle itself, this definition clearly depicts the state of liquid within the spray prior to impact, and is consistent with the definition of subcooling for all spray and jet studies. This is also a convenient definition for the user of a spray CHF correlation who has no means of determining a priori the temperature of liquid elsewhere in the system. In any case, the present study concerns cooling via a nozzle in close proximity

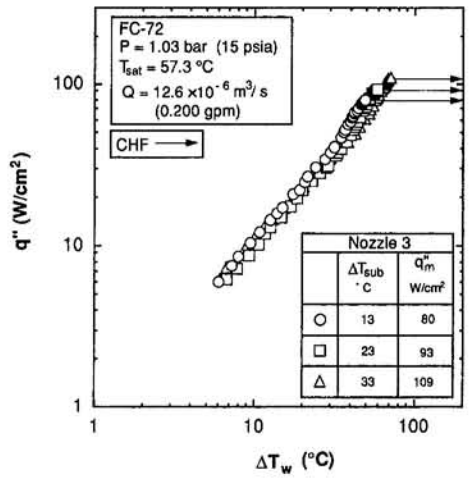

Fig. 10 Effect of subcooling on nozzle 3 boiling curve

to the surface, so any temperature changes in the liquid are expected to be quite small.

Unlike the water data of Mudawar and Valentine, the present study is concerned with intense cooling of a small square heater. It is postulated that CHF would commence at the outer edge of the spray impact area (which just inscribes the square heater), where volumetric flux is a minimum, and propagate inward in an unstable manner. Thus, critical heat flux at the outer edge, $q''_{m,p}$, can be related to the standard definition of CHF for the entire surface (i.e., q''_m) by the relation

$$q''_{m,p} = \frac{L^2}{\frac{\pi}{4} L^2} q''_m. \qquad (12)$$

The volumetric flux at the outer edge of the impact area can be related to the impact area's mean volumetric flux ($\overline{Q''} = Q/(\pi L^2/4)$) by setting $H = (L/2)/\tan(\theta/2)$ and $r = L/2$ in Eq. (8),

$$\frac{Q''}{\overline{Q''}} = \tfrac{1}{2}(1 + \cos(\theta/2))\cos(\theta/2). \qquad (13)$$

Figure 11 shows CHF data for FC-72 and FC-87 and the three full cone spray nozzles can be fitted over broad ranges of flow rate and subcooling according to the equation

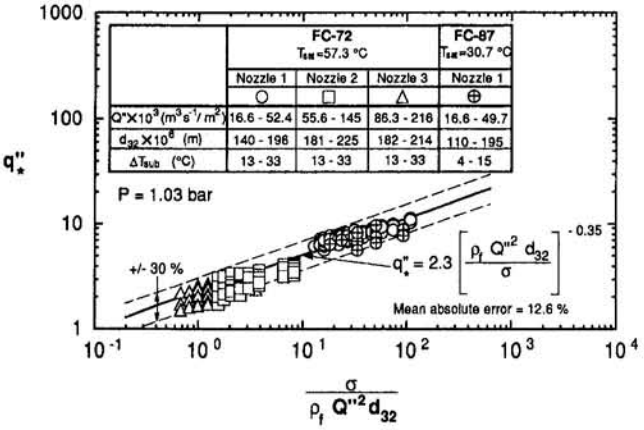

Fig. 11 Correlation of CHF data

$$q''_* \equiv \frac{\dfrac{q''_{m,p}}{\rho_g h_{fg} Q''}}{\left(\dfrac{\rho_f}{\rho_g}\right)^{0.3}\left[1 + 0.0019\,\dfrac{\rho_f c_{p,f}\Delta T_{sub}}{\rho_g h_{fg}}\right]}$$

$$= 2.3\left[\frac{\rho_f Q''^2 d_{32}}{\sigma}\right]^{-0.35} \quad (14)$$

with a mean absolute error of 11.5 percent.

As indicated earlier, CHF was measured experimentally when the heater thermocouple detected a sudden unsteady rise in the heater temperature. This is a true measure for CHF considering the small size of the heater used in the present study. The hypothesis of a CHF commencing from the outer edge and propagating inward is a description of the trigger point for CHF and the subsequent process of attainment of burnout over the entire heater surface. It is important to emphasize all these events occur at the same electrical power input. Thus, while the central thermocouple detects the temperature rise as it occurs at the center, it does so at the same power setting responsible for the onset of CHF along the outer edge, delayed very briefly by a combination of heat diffusion resistance within the heater block and the propagation speed of the dryout front. Because of their construction and high-conductivity materials, the applications for which the present study is intended (e.g., electronic and laser devices), tend to respond essentially as a lumped mass once the conditions for CHF have been attained.

Combining Eqs. (12)–(14) yields another more convenient form of the CHF correlation relating q''_m to $\overline{Q''}$:

$$\frac{q''_m}{\rho_g h_{fg} \overline{Q''}} = 1.467[(1 + \cos(\theta/2))\cos(\theta/2)]^{0.3} \times \left(\frac{\rho_f}{\rho_g}\right)^{0.3}\left[\frac{\rho_f \overline{Q''}^2 d_{32}}{\sigma}\right]^{-0.35}\left[1 + 0.0019\,\frac{\rho_f c_{p,f}\Delta T_{sub}}{\rho_g h_{fg}}\right]. \quad (15)$$

To predict CHF using Eq. (15), each nozzle has to be first tested to determine its flow characteristics (ΔP, Q, d_0, θ). These characteristics influence mean volumetric flux ($\overline{Q''}$), Sauter mean diameter (d_{32}), and optimum nozzle-to-surface distance (H) for a given heater length (L). Using Eq. (3) precludes having to perform any costly drop sizing experiments for each spray nozzle and operating pressure.

6 Conclusions

This study focused on optimizing CHF for spray cooling of a small heated surface. The key findings are as follows:

1 Volumetric flux is fairly uniform along any spherical surface centered at the spray orifice and confined by the spray angle. A theoretical model based on this assumption was developed that projects the uniform flux of the spherical surface onto the flat surface of the heater. This model shows volumetric flux is greatest at the center of the spray and decays radially toward the outer edge of the impact area.

2 New sampling techniques were developed to investigate the volumetric flux distribution across a flat surface. These techniques verified the accuracy of the theoretical volumetric flux distribution model.

3 Unlike jets, sprays produce drastically different cooling performances for the same nozzle and same flow rate depending upon the nozzle-to-surface distance. Therefore, this distance should be carefully selected to ensure both repeatability and predictability of cooling performance, especially near CHF.

4 Experiments revealed that when the nozzle-to-surface distance is very small, only a small fraction of the heater surface is directly impacted by the spray and the corresponding CHF is relatively small. Small CHF values are also encountered when the nozzle-to-surface distance is too large because a fraction of the spray liquid would fail to impact the heater surface and is, therefore, wasted. CHF is a maximum when the spray impact area just inscribes the square surface of the heater. Thus, the appropriate nozzle-to-surface distance can be easily determined knowing only the size of the heater and the spray angle.

5 A new correlation was developed for full cone sprays that accurately predicts CHF for different nozzles over broad ranges of flow rate and subcooling.

Acknowledgments

Financial support for this work by IBM is greatly appreciated. The authors also thank 3M Company for donating Fluorinert samples, and Spraying Systems Company for both donating spray nozzles and assisting with the spray droplet sizing.

References

Bolle, L., and Moureau, J. C., 1976, "Spray Cooling of Hot Surfaces: A Description of the Dispersed Phase and a Parametric Study of Heat Transfer Results," *Two Phase Flow Heat Transfer, Proceedings of NATO Advanced Study Institute*, Vol. 3, Washington, DC, pp. 1327–1346.

Estes, K. A., 1994, "Critical Heat Flux in Spray Cooling and Jet Impingement Cooling of Small Targets," Master's Thesis, School of Mechanical Engineering, Purdue University, West Lafayette, IN.

Hall, D. D., and Mudawar, I., 1995, "Experimental and Numerical Study of Quenching Complex-Shaped Metallic Alloys With Multiple, Overlapping Sprays," *International Journal of Heat and Mass Transfer*, Vol. 38, pp. 1201–1216.

Lefebvre, A. H., 1989, *Atomization and Sprays*, Hemisphere Publishing Corporation, New York.

Monde, M., Kusuda, H., and Uehara, H., 1980, "Burnout Heat Flux in Saturated Forced Convection Boiling With Two or More Impinging Jets," *Transactions of JSME*, Vol. 46, pp. 1834–1843.

Moriyama, A., Araki, K., Yamagami, M., and Mase, K., 1987, "Local Heat Transfer Coefficient in Spray Cooling a Hot Surface," *Proc. 15th Japanese Conference on Liquid Atomization and Spray Systems*, Vol. 28, Tokyo, Japan, pp. 104–109.

Mudawar, I., and Valentine, W. S., 1989, "Determination of the Local Quench Curve for Spray-Cooled Metallic Surfaces," *Journal of Heat Treating*, Vol. 7, pp. 107–121.

Mudawar, I., and Deiters, T. A., 1994, "A Universal Approach to Predicting Temperature Response of Metallic Parts to Spray Quenching," *International Journal of Heat and Mass Transfer*, Vol. 37, pp. 347–362.

Toda, S., 1972, "A Study in Mist Cooling," *Transactions of JSME*, Vol. 38, pp. 581–588.

Watchers, L. H. J., Smulders, L., Vermeulen, J. R., and Kleiweg, H. C., 1966, "The Heat Transfer From a Hot Wall to Impinging Mist Droplets in the Spheroidal State," *Chemical Engineering Science*, Vol. 21, pp. 1231–1238.